Available online at www.sciencedirect.com
ScienceDirect
Trans. Nonferrous Met. Soc. China 27(2017) 1327−1337
Transactions of Nonferrous Metals Society of China
www.tnmsc.cn

Optimization of deformation parameters of dynamic recrystallization for 7055 aluminum alloy by cellular automaton

Tao ZHANG[1], Shi-hong LU[1], Yun-xin WU[2], Hai GONG[2]

1. College of Mechanic and Electrical Engineering, Nanjing University of Aeronautics and Astronautics, Nanjing 210016, China;
2. School of Mechanical and Electrical Engineering, Central South University, Changsha 410083, China

Received 6 April 2016; accepted 22 November 2016

Abstract: In order to simulate the microstructure evolution during hot compressive deformation, models of dynamic recrystallization (DRX) by cellular automaton (CA) method for 7055 aluminum alloy were established. The hot compression tests were conducted to obtain material constants, and models of dislocation density, nucleation rate and recrystallized grain growth were fitted by least square method. The effects of strain, strain rate, deformation temperature and initial grain size on microstructure variation were studied. The results show that the DRX plays a vital role in grain refinement in hot deformation. Large strain, high temperature and small strain rate are beneficial to grain refinement. The stable size of recrystallized grain is not concerned with initial grain size, but depends on strain rate and temperature. Kinetic characteristic of DRX process was analyzed. By comparison of simulated and experimental flow stress–strain curves and metallographs, it is found that the established CA models can accurately predict the microstructure evolution of 7055 aluminum alloy during hot compressive deformation.

Key words: 7055 aluminum alloy; cellular automaton; dynamic recrystallization; hot compression; grain refinement

1 Introduction

Aluminum alloy plates with high strength and high toughness are widely used in main frames, wing boxes, stringers and other key components of aircraft. 7055 aluminum alloy is an ultra-high strength aluminum alloy developed by Alcoa Company in the United States, which was used in the aircraft airfoil of B777. The use of aluminum alloy plates makes about 635 kg reduction compared with the designed mass in B777 [1,2]. With the development of manufacture of aircraft, higher requirements of the properties (strength, toughness, ductility and corrosion resistance) of aluminum alloy were put forward. Mechanical properties strongly depend on the internal microstructure of the material. It is known that finer grain is beneficial to improving the mechanical properties. Therefore, control of the microstructure evolution during hot deformation plays a vital role in the optimization of the mechanical properties. Dynamic recrystallization (DRX) is a common phenomenon in the hot plastic deformation and it has a great influence on the microstructure and mechanical properties of the material. Many models and methods have been applied to studying the DRX process in metal material, such as empirical models [3], method phase field (PF) [4,5], Monte-Carlo method (MC) [6−8] and cellular automaton method (CA) [9,10]. The values of DRX fraction and grain size can be calculated in empirical models fitted by experiment, while the grain morphology cannot be simulated. The disadvantages of PF and MC are that model parameters are difficult to be determined and the computing efficiency for huge amount of calculation is low. Compared with other methods, the evolution law can be applied to physical system in discrete space-time and the CA method is more flexible in simulating the DRX process. HESSELBARTH and GOBEL [11] first studied the static recrystallization by CA method and the effects of neighbor types and nucleation types on DRX kinetics were studied. The simulation of DRX process was first studied by GOETZ and SEETHARAMAN [12] and the processes of dynamic recovery, nucleation and grain growth were taken into account. SHI et al [13] established a modified CA model to simulate three-

Foundation item: Projects (51175257, 51405520) supported by the National Natural Science Foundation of China
Corresponding author: Tao ZHANG; Tel: +86-15250997258; E-mail: 297zhangtao@nuaa.edu.cn
DOI: 10.1016/S1003-6326(17)60154-7

dimensional dendrite growth. JIN et al [14] put forward an adaptive response surface method to acquire identification of nucleation parameter for cellular automaton model. RAABE [15−17] established a probabilistic CA model determined by driving force on the basis of deterministic CA model. The combination of physical metallurgy principle and random algorithms was applied in CA model by DING and GUO [18,19]. Effects of strain rate and temperature on the flow stress and DRX process in hot deformation for different metals were studied [20].

However, studies on prediction of the microstructure evolution during DRX process of aviation material, especially for 7055 aluminum alloy, were rarely published. The effects of deformation parameters (strain, strain rate, temperature and initial grain size) on DRX process were not studied comprehensively in previous researches and they need to be further studied as the DRX behavior varies under different deformation conditions. What is more, the kinetic rule of DRX can describe the DRX speed and the Avrami exponent is a vital parameter to describe the accuracy of the CA models. In this study, the hot compression experiments for 7055 aluminum alloy on Gleeble 3180 machine were conducted and models of cellular automaton were built. The equations of dislocation density, nucleation rate and grain growth were fitted by least square method. The microstructure evolution during hot deformation by CA was simulated and the effects of strain, strain rate, temperature and initial grain size on the microstructure were investigated. Simulated microstructures by CA method were compared with experimental isothermal compression tests. In addition, kinetic equation of DRX was analyzed and Avrami exponent agrees well with the theoretical value.

2 Models of cellular automaton

DRX is a common phenomenon when the dislocation density reaches the critical value during hot deformation. CA models are adopted to describe the relationship between the flow stress, DRX fraction and grain size. In CA model, the complex object is divided into cells discrete in time and space, and complex issues can be described through random algorithm and transition rules between the cell and its neighborhood. Status values of each cell are updated at each time step according to the transition rules between the cell and its Moore neighborhood. The CA models established in this study contain four modules: initial microstructure module, dislocation density module, nucleation rate module and grain growth module, which are described as follows.

2.1 Model of initial microstructure

The homogenization treatment should be conducted before the thermal deformation for 7055 aluminum alloy ingot casting. The objective of homogenization treatment is to decrease microsegregation and acquire super saturated solid solution in the casting process. After homogenization treatment, equiaxial structure with uniform grain size can be obtained. In CA model, the nucleation points were spread uniformly into the simulation zone and they grew into equiaxial grains in all directions with the same probability. Figure 1 shows the initial microstructure of 7055 aluminum alloy with the grain sizes of 100 and 150 μm, respectively.

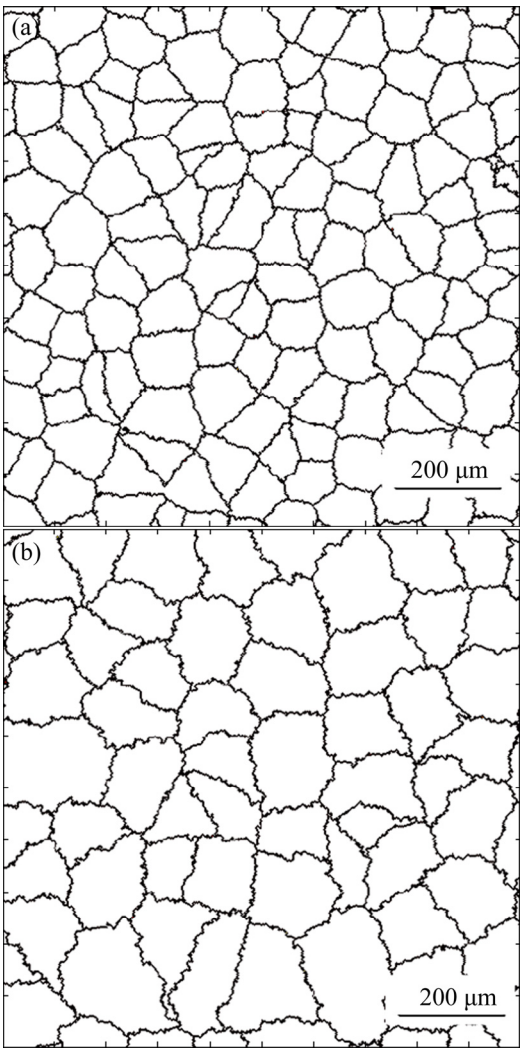

Fig. 1 Initial microstructure of 7055 aluminum alloy with grain sizes of 100 μm (a) and 150 μm (b)

2.2 Model of dislocation density

The dislocation density in material plays a vital role in microstructure evolution during DRX. The variation of dislocation density depends on two processes: work hardening and dynamic softening. Dislocation density is increased with the increase of strain during hot

deformation; meanwhile, it is decreased for dynamic recovery (even dynamic recrystallization) under high temperature. Usually, the dislocation density with respect to strain was described in Eqs. (1)−(3):

$$\frac{\mathrm{d}\rho}{\mathrm{d}\varepsilon}=k_1\sqrt{\rho}-k_2\rho \tag{1}$$

$$k_1=2\theta_0/(\alpha\mu b) \tag{2}$$

$$k_2=2\theta_0/\sigma_s \tag{3}$$

where ρ is the dislocation density, ε is the true strain, k_1 is the coefficient of work hardening, k_2 is the coefficient of dynamic softening, α is the dislocation interaction term, μ is the shear modulus, b is the modulus of Burger's vector, σ_s is the saturated flow stress. $\theta_0=\mathrm{d}\sigma/\mathrm{d}\varepsilon$ is the work hardening rate that can be obtained from the slope of the experimental flow stress−strain curve [21,22]. The θ_0 is the function of strain rate and absolute temperature and can be described with Eq. (4).

$$\theta_0=A\dot{\varepsilon}^B\exp(C/T) \tag{4}$$

where A, B and C are material constants.

2.3 Model of nucleation rate

During hot deformation, the variation of dislocation density is calculated by Eq. (1), dynamically recrystallized grain started to nucleate in a rate ($\dot{n}$) when the dislocation density exceeded critical value ρ_c for DRX. The nucleation rate ($\dot{n}$) is the function of the strain rate, temperature and active energy by DING and GUO [18,19].

$$\dot{n}=C\dot{\varepsilon}^m\exp\left(\frac{-Q_{act}}{RT}\right) \tag{5}$$

where C is the material constant, m is the sensitivity coefficient of strain rate and is set as 1 in DING's model, Q_{act} is the active energy and R is the mole gas constant.

Critical dislocation density (ρ_c) considering the energy change for DRX can be calculated by Eqs. (6)−(8):

$$\rho_c=\left(\frac{20\gamma_m\dot{\varepsilon}}{3blM\tau^2}\right)^{1/3} \tag{6}$$

$$\frac{\sigma_s l}{\mu b}=K \tag{7}$$

$$\tau=\alpha\mu b^2 \tag{8}$$

where γ_m is the grain boundary (GB) energy of high angle boundary, l is the dislocation mean free path, τ is the dislocation line energy, M is the GB mobility, σ_s is the saturated flow stress, K is a constant and its value is 10 for most metal materials.

2.4 Model of grain growth

After the nucleation of DRX, there is a large difference between the dislocation densities of the dynamic recrystallized grain and the matrix. The dislocation densities of newly DRX nuclei are equal to the initial value, while the dislocation density of the matrix increases with the ascending strain. The dislocation density difference provides the thermo-dynamic driving force for the growth of the dynamic recrystallized grains. It is assumed that the moving velocity of a GB (v) is proportional to the pressure (p) and the GB mobility and it can be expressed in Eqs. (9)−(12) [23]:

$$v=Mp \tag{9}$$

$$M=\frac{b}{kT}\lambda D_b\exp\left(\frac{-Q_b}{RT}\right) \tag{10}$$

$$p=\tau\Delta\rho-\frac{2\gamma_i}{r_i} \tag{11}$$

$$\gamma_i=\begin{cases}\gamma_m, & \theta_i>\theta_m\\ \gamma_m\dfrac{\theta_i}{\theta_m}\left[1-\ln\left(\dfrac{\theta_i}{\theta_m}\right)\right], & \theta_i\le\theta_m\end{cases} \tag{12}$$

where k is Boltzmann constant, λ is the thickness of characteristic GB, D_b is the boundary self-diffusion coefficient, Q_b is the boundary diffusion activation energy, $\Delta\rho$ is the dislocation density difference between the recrystallized grain and the matrix, γ_i is the GB energy and θ_i is the misorientation between the ith recrystallized grain and its neighboring grain.

3 Experimental

3.1 Experiment procedures

The hot compression tests for 7055 aluminum alloy were conducted for the purposes of obtaining material constants in the CA simulation and validation for accuracy of CA model. The material is 7055 aluminum alloy ingot casting after homogenization treatment and its compositions (mass fraction, %) 6.7Zn−2.6Mg−2.6Cu−0.15Fe−0.13Zr−0.12Si−0.06Ti. The homogenization treatment process was conducted as follows: the material was heated to 470 °C from room temperature and held for 24 h to obtain heat balance between the surface and the center, then cooled down with the heating furnace. Cylindrical specimens were machined with a diameter of 10 mm and a height of 15 mm. The hot compression tests were conducted on a Gleeble−3180 thermo-simulation machine at four different temperatures (300, 350, 400 and 450 °C) and four different strain rates (0.01, 0.1, 1 and 10 s^{-1}). The reduction in height is 50% in the end and the specimens were quenched immediately after the deformation to reserve high temperature deformed microstructure.

In the compression test, the deformation in the cylindrical specimen is not uniform; there are large deformation zone, small deformation zone (near the upper and lower surfaces) and non-deformation zone. However, the area of large deformation zone is much larger than that of other zones on axial section. Small strain has little effect on work hardening and it cannot induce dynamic recrystallization. In small deformation zone, the microstructure change is not obvious and it is similar to the cast structure. In CA models and compression test, the microstructure evolution of the position near the center of the cross section of the cylindrical specimen was studied because most regions of the cross section are large deformation zones.

3.2 Experimental results

True stress−true strain curves of 7055 aluminum alloy under different compression conditions are depicted in Fig. 2. It is obvious that the true stress is sensitive to deformation temperature and strain rate. The flow stress increases with the increase of strain rate and decrease of temperature. Through true stress−true strain curves, saturated flow stress (σ_s) for 7055 aluminum alloy can be expressed in Eq. (13):

$$\sigma_s = 68.03\ln\{[Z/(6.12\times10^9)]^{1/5.22} + [(Z/(6.12\times10^9))^{2/5.22}+1]^{1/2}\}$$
$$Z = \dot{\varepsilon}\exp[1.36382\times10^5/(RT)] \quad (13)$$

The work hardening rate (Z) is the function of strain rate and absolute temperature and Figs. 3 and 4 show the relationship between $\ln\theta_0$−$\ln\dot{\varepsilon}$ and $\ln\theta_0$−$1/T$. The values of B and C can be obtained from the average slope of the four lines by least square method. The mean values of B and C were computed as 0.1014 and 1913.7, respectively and the work hardening rate for 7055 aluminum alloy is shown in Eq. (14):

$$\theta_0 = 182\dot{\varepsilon}^{0.1014}\exp(1913.7/T) \quad (14)$$

According to true stress−true strain curves and metallographic structure of 7055 aluminum alloy, the nucleation rate can be calculated by [19]:

$$X_d = \dot{n}\frac{\varepsilon}{\dot{\varepsilon}}\frac{4}{3}\pi D_d^3 \quad (15)$$

where X_d is the DRX fraction, $\dot{n}$ is the nucleation rate, and D_d is the mean size of recrystallized grain.

The relationship between $\ln\dot{n}$ −$1/T$ is shown in Fig. 5. The value of Q_{act} can be obtained from the average

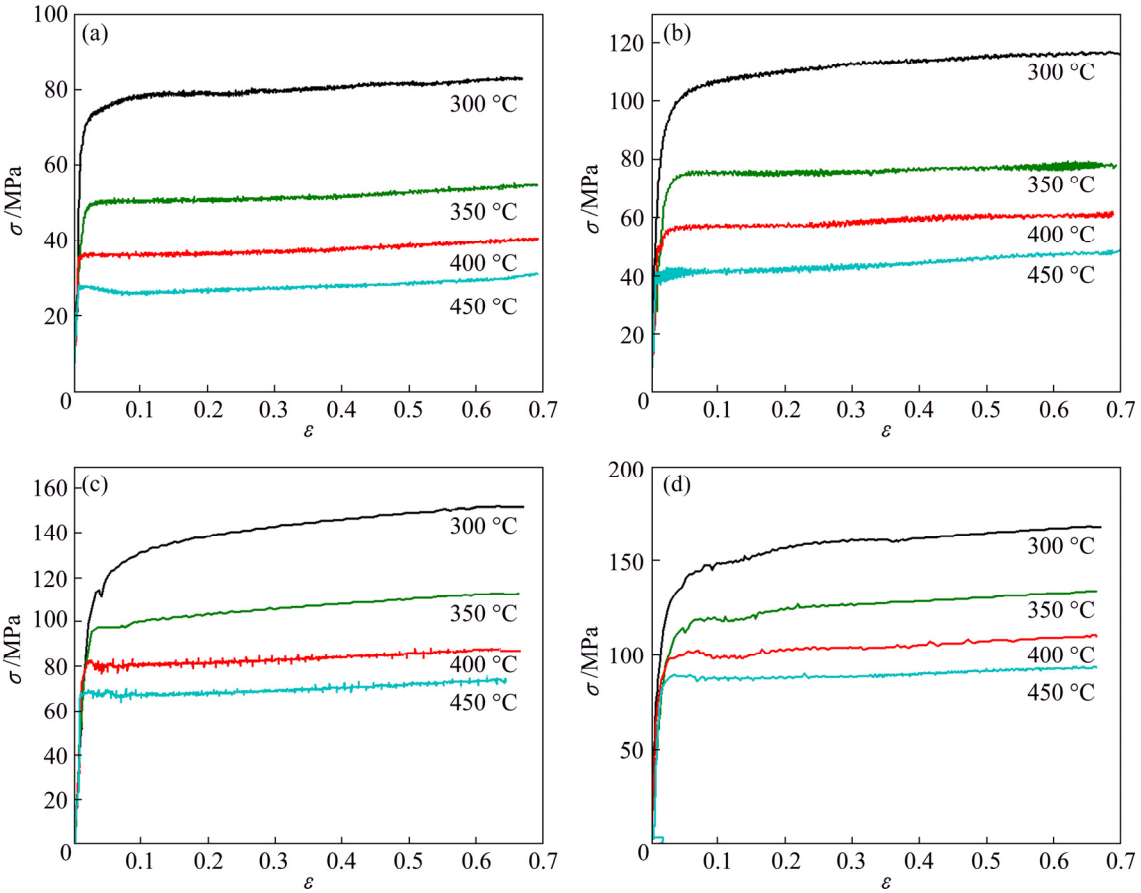

Fig. 2 True stress−strain curves of 7055 aluminum alloy under different deformation conditions: (a) $\dot{\varepsilon}$ = 0.01 s^{-1}; (b) $\dot{\varepsilon}$ = 0.1 s^{-1}; (c) $\dot{\varepsilon}$ = 1 s^{-1}; (d) $\dot{\varepsilon}$ = 10 s^{-1}

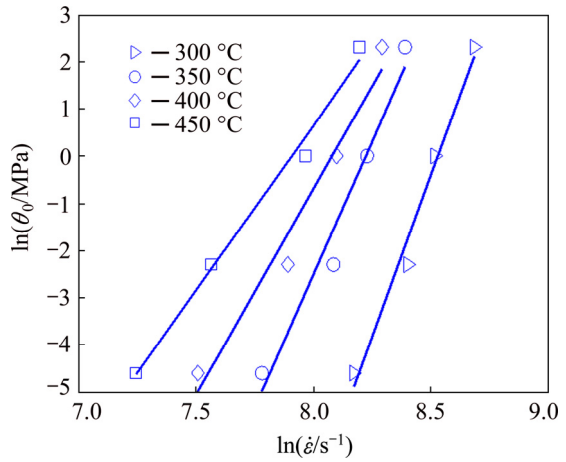

Fig. 3 Relationship between $\ln\theta_0$ and $\ln\dot{\varepsilon}$

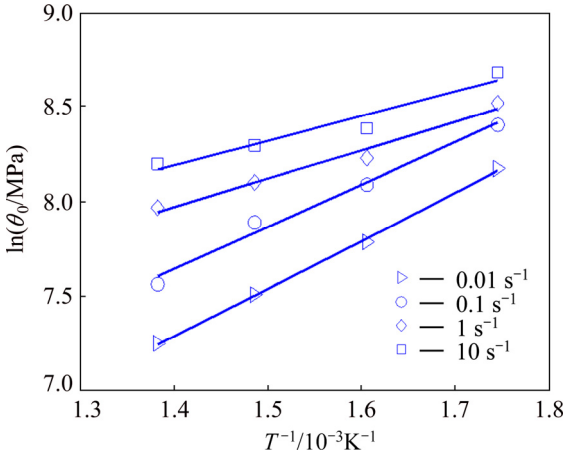

Fig. 4 Relationship between $\ln\theta_0$ and $1/T$

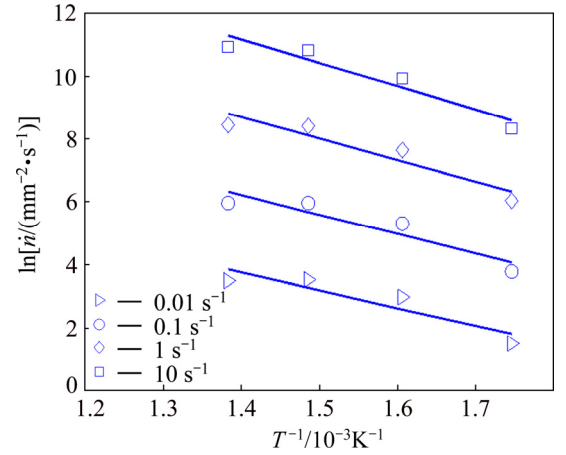

Fig. 5 Relationship between $\ln\dot{n}$ and $1/T$

slope of the four lines. Constant C was optimized by Fminunc function in MATLAB to improve the accuracy and the objective function is shown in Eq. (16). Therefore, the nucleation rate for 7055 aluminum alloy is expressed in Eq. (17).

$$f(C)=\min\left[\dot{n}_e-C\dot{\varepsilon}\exp\left(\frac{-Q_{act}}{RT}\right)\right]^2 \quad (16)$$

$$\dot{n}=C\dot{\varepsilon}\exp[-73220.3/(RT)] \quad (17)$$

where C is equal to 2.3966×10^9 $m^{-2}\cdot s^{-1}$.

4 Results and discussion

The simulation of microstructure evolution in DRX was conducted by CA method and the material parameters for 7055 aluminum alloy are shown in Table 1. The simulation area is 1 mm × 1 mm and corresponds to a point in the macro level, which is divided into a mesh with 500 × 500 square lattice in CA model. According to experimental results, the grain size of initial microstructure is set as 100 μm. The effects of strain, temperature, strain rate and initial grain size on DRX process were studied.

Table 1 Material parameters for 7055 aluminum alloy

Parameter	Value
b/m	2.6×10^{-10}
μ/GPa	26
γ_m/(J·m^{-2})	0.231
Q_b/(J·mol^{-1})	142000
λD_b/(m^3·s^{-1})	5×10^{-14}
k/(J·K^{-1})	1.38×10^{-23}

4.1 Effect of strain

Figure 6 shows the CA simulated microstructure evolution at different strains, temperature of 450 °C and strain rate of 0.01 s^{-1}, in which the white regions represent the matrix and the color regions represent dynamic recrystallized grain. The DRX nuclei were first formed at the grain boundary for its high energy and the size of the recrystallized grain increases with ascending strain. The DRX nuclei can grow into recrystallized grains with certain size by absorbing the initial microstructure to make it into dynamic recrystallized grains. The deformation energy inside the material provides thermodynamic driving force for this absorption process. The effect of strain on DRX parameters is shown in Fig. 7. With the increase of strain, the DRX fraction increases sharply firstly for small strains and then slowly; the mean size of recrystallized grain increases to a peak value and then keeps steady; the average grain size decreases. As strain increases, the dislocation density and deformation energy of the material both increase, as a result, the number of DRX nuclei increases. Therefore, the DRX fraction and the mean size of recrystallized grain increase in the grain growth process for large number of DRX nuclei; the average grain size obviously decreases as the grain size of DRX grain is quite small to the matrix. However, further increase of strain has little effect on DRX

parameters because the dislocation density difference between the recrystallized grain and the matrix decreases as both of them will reach a stable value. It is easily seen that DRX plays a significant role in grain refinement and the average grain size is decreased from 100 to 48.2 μm at DRX fraction of 86%.

4.2 Effect of strain rate

Figure 8 shows the CA simulated microstructure evolution at different strain rates, temperature of 450°C and strain of 0.693. Large number of DRX nuclei were formed at the grain boundary and the nucleation rate is larger for higher strain rate according to Eq. (17). However, the DRX nuclei grow into recrystallized grains with certain sizes for small strain rate (≤0.1 s^{-1}), but for large strain rate (>0.1 s^{-1}), the grain sizes of the recrystallized grains are quite small and nearly equal to those of the nuclei. The effect of strain rate on the DRX parameters is shown in Fig. 9. With the decrease of strain rate, the DRX fraction and the mean size of recrystallized grain are increased, while the average grain size is decreased. As strain rate increases, the number of DRX nuclei is increased, however, the DRX nuclei do not have sufficient time to grow into recrystallized grain for large strain rate. As a result, the portion of the matrix absorbed by the DRX nuclei is

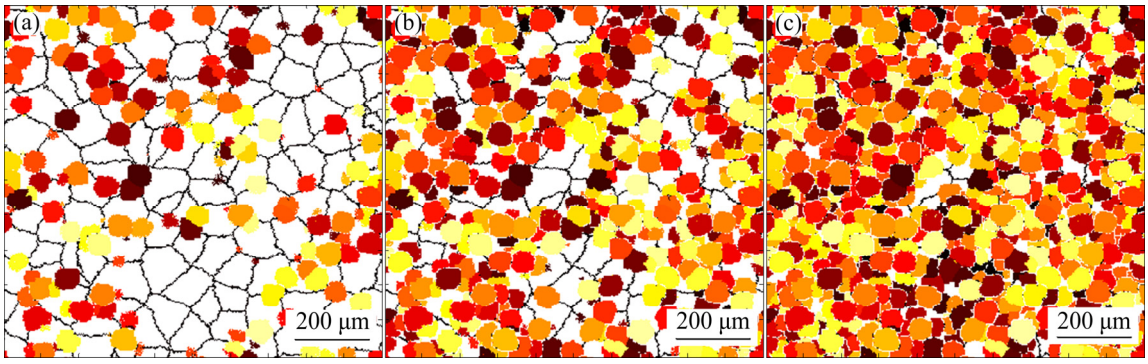

Fig. 6 Simulated microstructure evolution at different strains, temperature of 450 °C and strain rate of 0.01 s^{-1}: (a) ε=0.18; (b) ε=0.35; (c) ε=0.69

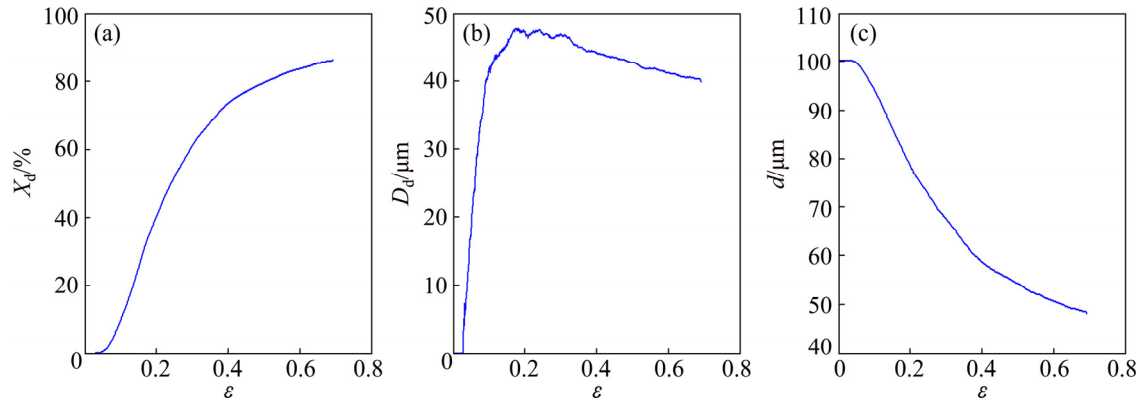

Fig. 7 Effect of strain on recrystallization fraction (X_d) (a), mean size of recrystallized grain (D_d) (b) and average grain size (d) (c)

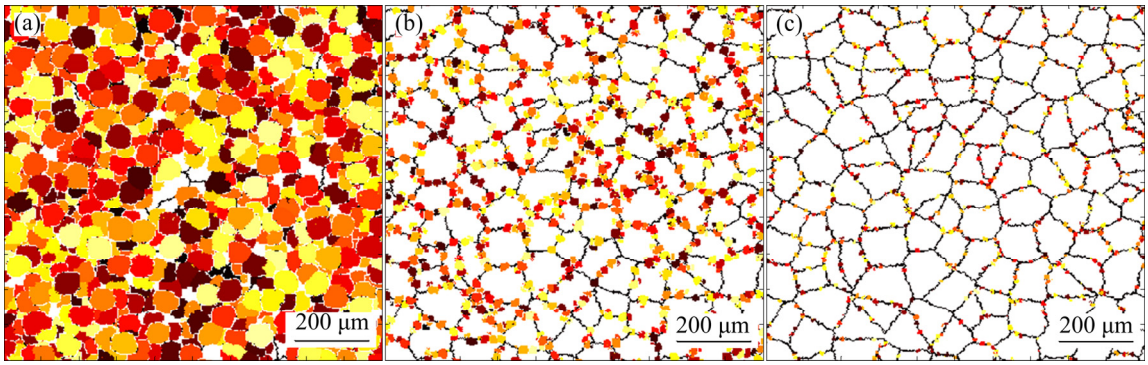

Fig. 8 Simulated microstructure evolution at different strain rates, temperature of 450 °C and strain of 0.693: (a) $\dot{\varepsilon}$=0.01 s^{-1}; (b) $\dot{\varepsilon}$=0.1 s^{-1}; (c) $\dot{\varepsilon}$=1 s^{-1}

decreased in the grain growth process and the DRX fraction is smaller for larger strain rates. From Fig. 9(c), the variation of average grain size is sensitive to the strain rate and small strain rate is beneficial to the grain refinement. It is obvious that the average grain size is 48.2 μm for 0.01 s^{-1} and 97.4 μm for 10 s^{-1}. Meanwhile, it can be found that the incubation time before DRX decreases with descending strain rate as the DRX fraction increases sharply at small strain for small strain rate. According to Eq. (6), smaller strain rate results in smaller critical dislocation density, therefore, the DRX process took place more quickly at smaller strain rate.

4.3 Effect of temperature

Figure 10 shows the CA simulated microstructure evolution at different temperatures, strain rate of 0.01 s^{-1} and strain of 0.693. More DRX nuclei were formed at higher temperatures, which is consistent with Eq. (6). With the increase of temperature, the DRX fraction and the mean size of recrystallized grain are increased, while the average grain size is decreased, which is shown in Fig. 11. On one hand, higher temperature enhances the thermally activated motion of atoms and molecules in the materials and the nuclei process of DRX. On the other hand, higher temperature increases the deformation

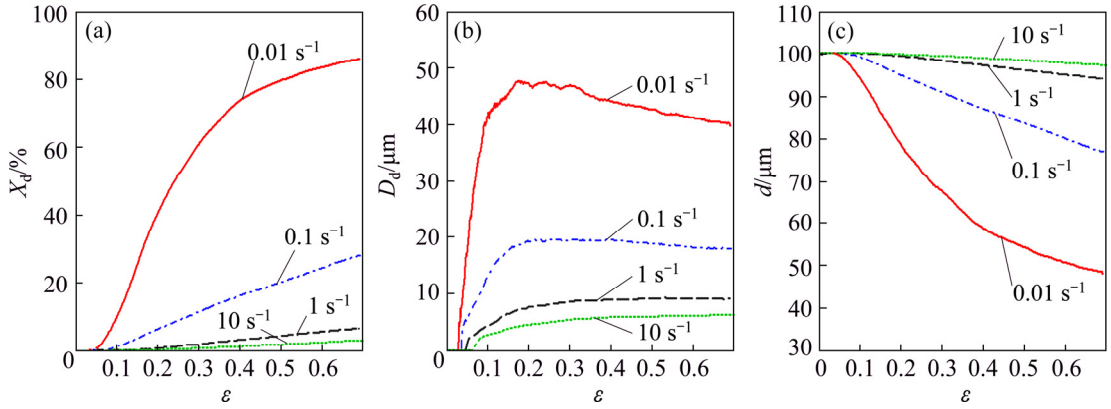

Fig. 9 Effect of strain rate on recrystallization fraction (a), mean size of recrystallized grain (b) and average grain size (c)

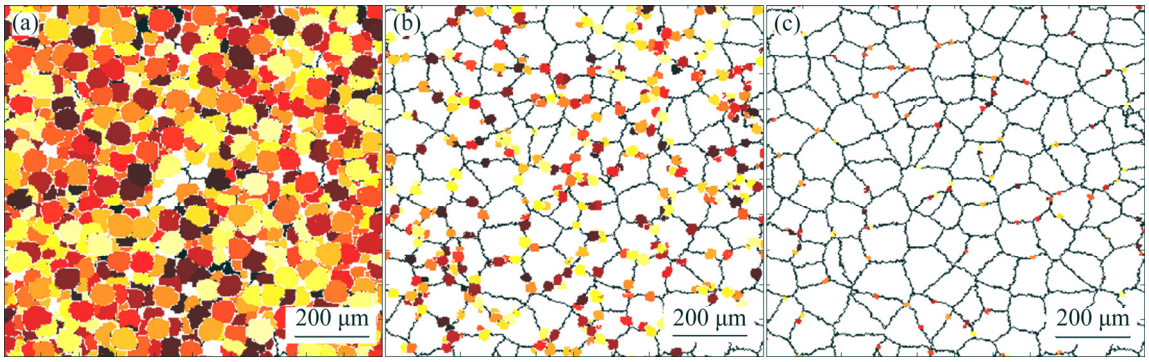

Fig. 10 Simulated microstructure evolution at different temperatures, strain of 0.693 and strain rate of 0.01 s^{-1}: (a) 450 °C; (b) 400 °C; (c) 350 °C

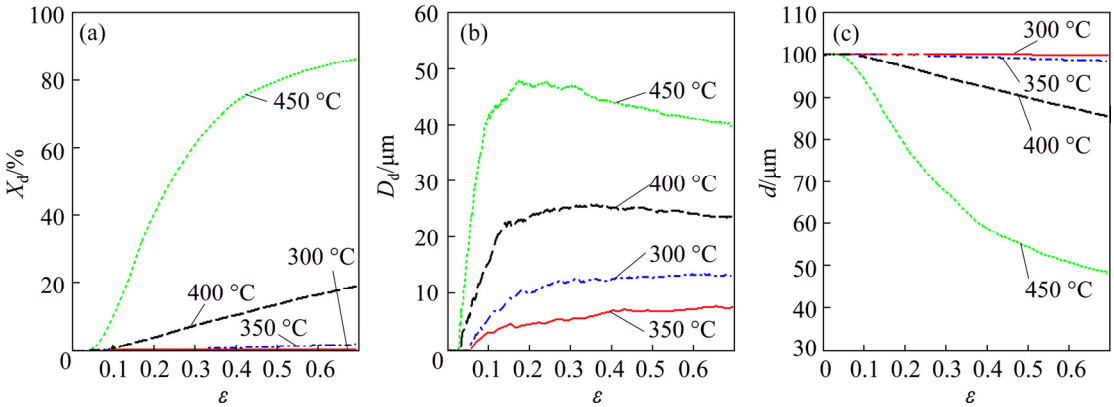

Fig. 11 Effect of temperature on recrystallization fraction (a), mean size of recrystallized grain (b) and average grain size (c)

energy and enhances the thermodynamic driving force for the growth process of DRX. Therefore, more DRX nuclei and stronger growth process result in higher DRX fraction. Meanwhile, higher temperature will change the state of the internal microstructure of the material by accelerating the solubility of microelement into the matrix, thereby reducing the inhibition caused by the precipitation on DRX process. As is known, larger grain size can be generated at high temperatures; however, it is interesting that the average grain size decreases with ascending temperature. The average grain size is equal to the mean recrystallized grain size for fully dynamic recrystallization. In this study, for 7055 aluminum alloy, the mean recrystallized grain size is about 45 μm at 450 °C and 5 μm at 300 °C, while the DRX fractions are 86% and 0.2%, respectively. And the corresponding average grain sizes are 48.2 and 100 μm, which indicates that DRX fraction plays a dominant role in the grain refinement. The incubation time before DRX decreases with ascending temperature because of lower critical dislocation density at higher temperatures.

4.4 Effect of initial grain size

To study the effect of initial grain size on DRX parameters, three different values of 100, 150 and 200 μm were simulated by the method introduced in Section 2.1 and the results are shown in Fig. 12. With the increase of initial grain size, the DRX fraction is slightly decreased and the average grain size is increased, while the mean size of recrystallized grain keeps unchanged. The number of grain boundaries between the grains will be reduced for large initial grain size; therefore, the DRX nucleation position will be reduced in the given simulation zone. Less DRX nuclei will result in smaller DRX fraction and the average grain size is increased with ascending initial grain size due to incomplete DRX. The stable size of recrystallized grain is concerned with the saturated flow stress, which depends on the strain rate and temperature. It can be seen that the stable size of recrystallized grain has nothing to do with initial grain size in Eq. (18), which agrees with the simulation results in this study. Complete DRX will be generated for further increase of strain, in which the average grain size is equal to stable size of recrystallized grain and reaches the same value for different initial grain sizes.

$$\frac{\sigma_s}{\mu}\left(\frac{2R_d}{b}\right)^n = c \tag{18}$$

where R_d is the stable radius of recrystallized grain, n is a constant of 2/3 and c is a constant varied from 1 to 10.

4.5 Verification of CA model

The relationship between flow stress and average dislocation density can be described in Eq. (19) and the average dislocation density can be calculated in Eq. (20):

$$\sigma_{CA} = \alpha\mu b\sqrt{\bar{\rho}} \tag{19}$$

$$\bar{\rho} = \frac{1}{N}\sum_{i,j}\rho_{i,j} \tag{20}$$

where σ_{CA} is the simulated flow stress by CA, $\bar{\rho}$ is the average dislocation density, N is the total number of cells in CA model and $\rho_{i,j}$ is the dislocation density of single cell. The comparisons between CA simulated and experimental flow stresses are depicted in Fig. 13. The stable flow stress and rising rate of the curves agree with the experimental curves. The error between the simulated and experimental result is defined in Eq. (21) and the maximum error is 9.43% at 0.1 s^{-1} and 450 °C.

$$e = |\sigma_{CA} - \sigma_e| / \sigma_e \times 100\% \tag{21}$$

where σ_e is the experimental flow stress.

Figure 14 shows the comparisons between CA simulated and experimental metallographic structures under different deformation conditions by metallographic microscope. The average grain sizes of the experiment are 46.4, 74.3 and 95.2 μm for 0.01, 0.1 and 10 s^{-1} at 450 °C, while the CA simulated values are 48.2, 77 and 97.4 μm, respectively.

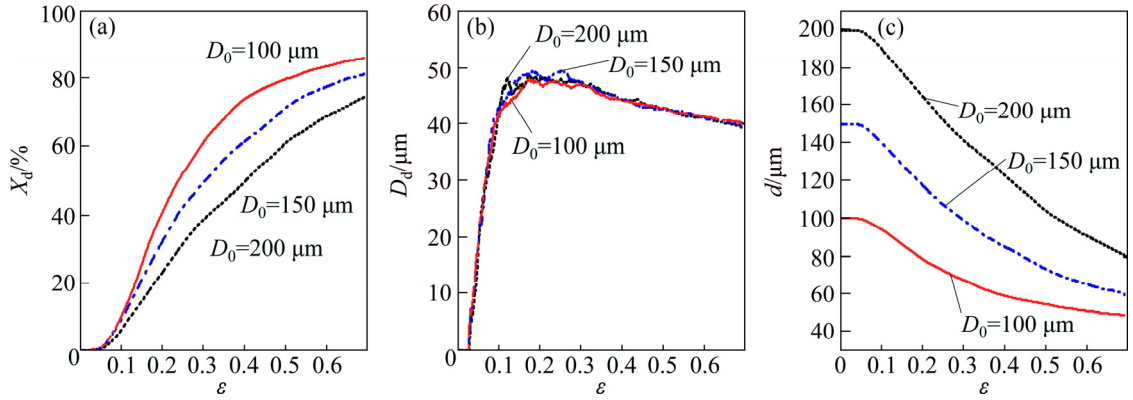

Fig. 12 Effect of initial grain size (D_0) on recrystallization fraction (a), mean size of recrystallized grain (b) and average grain size (c)

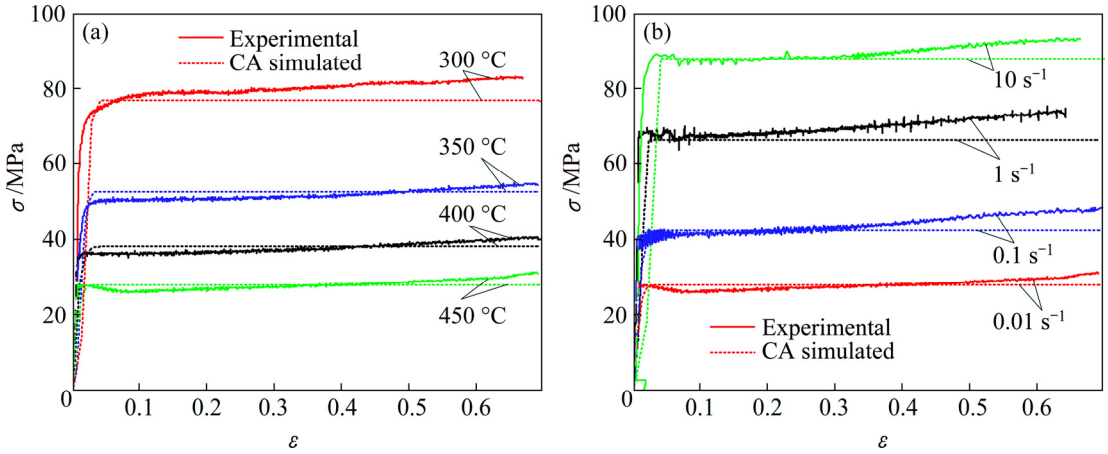

Fig. 13 Comparisons between CA simulated and experimental flow stresses: (a) $\dot{\varepsilon}=0.01\ s^{-1}$; (b) T=450 °C

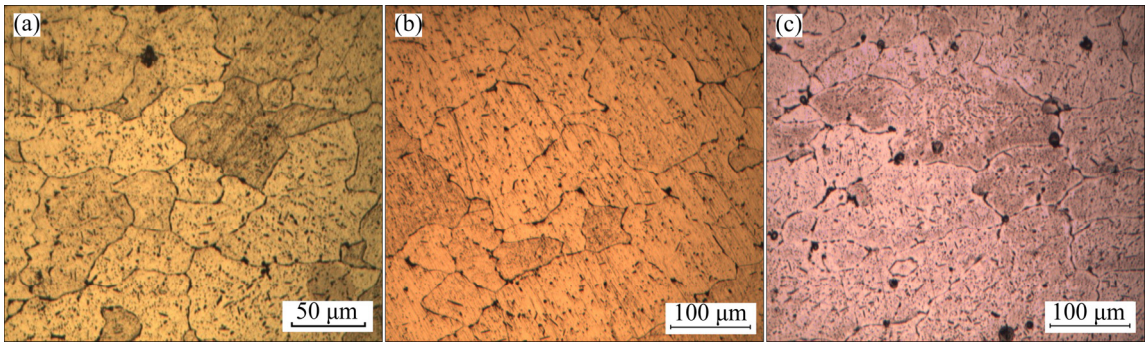

Fig. 14 Experimental microstructures at 450 °C and strain of 0.693: (a) $\dot{\varepsilon}$=0. 01 s^{-1}; (b) $\dot{\varepsilon}$=0.1 s^{-1}; (c) $\dot{\varepsilon}$=10 s^{-1}

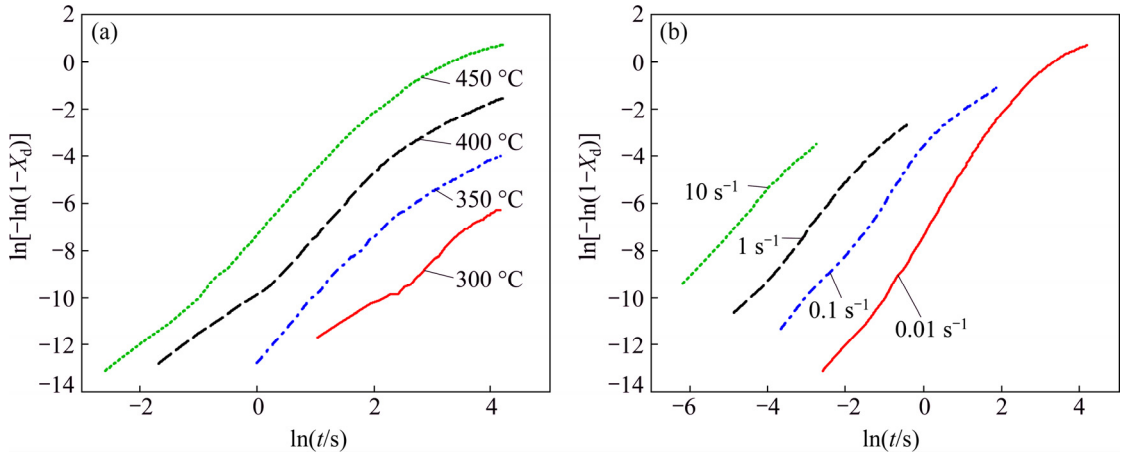

Fig. 15 Avrami curves for 7055 aluminum alloy at $\dot{\varepsilon}$=0.01 s^{-1} (a) and T=450 °C (b)

The DRX fraction is the function of deformation time and can be expressed by JMAK equation [24], which is shown in Eq. (20):

$$X_d = 1-\exp(-Bt^k) \quad (22)$$

where t is deformation time and k is Avrami exponent. Avrami exponent varies for different nucleation modes and model dimensions in CA. Nucleation modes consist of position saturated nucleation and constant rate nucleation and CA simulation dimensions consist of 2D and 3D. For 2D CA model, Avrami exponent is 2 for position saturated nucleation and 3 for constant rate nucleation, while the corresponding values are 3 and 4 in 3D model. Taking the logarithm of both sides of Eq. (22), the relationship between $\ln[-\ln(1-X_d)]$ and $\ln t$ is shown in Eq. (23) and Fig. 15. The value of k can be obtained from the average slope of the four lines by least square method. In this study, 2D CA models were built and position saturated nucleation was applied to the models. The mean value of k was computed as 1.91 at 0.01 s^{-1}

and 1.93 at 450 °C, respectively, which is quite close to the theoretical value.

$$\ln[-\ln(1-X_d)] = k\ln t + \ln B \quad (23)$$

5 Conclusions

1) Quantitative CA models coupling the metallurgical principles of DRX and the randomized algorithm were developed. The microstructure evolution under hot compression tests for different strain rates and temperatures was studied.

2) The work hardening rate, dislocation density model, nucleation rate model and grain growth model for 7055 aluminum alloy are established by the results from hot compression tests.

3) High strain, high temperature and small strain rate are beneficial to larger DRX fraction and smaller average grain size. Temperature of 400−450 °C and strain rate of 0.01−0. 1 s^{-1} are the desired deformation parameters for grain refinement of 7055 aluminum alloy.

4) The initial grain size has no effect on the size of recrystallized grain, which depends on strain rate and temperature.

5) The results in CA model agree with experimental results. The established CA model can provide guidance for the microstructure evolution under hot compression.

References

[1] STARKE E A, STALEY J T. Application of modern aluminum alloys to aircraft [J]. Progress in Aerospace Sciences, 1996, 32(2): 131−172.

[2] HEINZ A, HASZLER A, KEIDEL C. Recent development in aluminium alloys for aerospace applications [J]. Materials Science and Engineering A, 2000, 280(1): 102−107.

[3] LIN Yong-cheng, CHEN Ming-song, ZHONG Jue. Numerical simulation for stress/strain distribution and microstructural evolution in 42CrMo steel during hot upsetting process [J]. Computational Materials Science, 2008, 43(4): 1117−1122.

[4] CHEN Long-qing. Phase-field models for microstructure evolution [J]. Annual Review of Materials Research, 2002, 32(1): 113−140.

[5] MOELANS N, BLANPAIN B, WOLLANTS P. An introduction to phase-field modeling of microstructure evolution [J]. Calphad, 2008, 32(2): 268−294.

[6] PEZAK P, LUTON M J. A Monte Carlo study of the influence of dynamic recovery on dynamic recrystallization [J]. Acta Metallurgica et Materialia, 1993, 41(1): 59−71.

[7] HORE S, DAS S K, BANERJEE S, MUKHERJEE S. A multiscale coupled Monte Carlo model to characterize microstructure evolution during hot rolling of Mo-TRIP steel [J]. Acta Materialia, 2013, 61(19): 7251−7259.

[8] ZHANG Ji-xiang, WEN Hui, LIU Yun-teng. Monte Carlo model in metal recrystallization simulation [J]. Journal of Shanghai Jiao Tong University(Science), 2011, 16: 337−342.

[9] LAN Y J, LI D Z, LI Y Y. Mesoscale simulation of ferrite transformation from deformed austenite during continuous cooling in a C−Mn steel using a cellular automaton method [J]. Computational Materials Science, 2005, 32(2): 147−155.

[10] LEE H W, IM Y T. Cellular automata modeling of grain coarsening and refinement during the dynamic recrystallization of pure copper [J]. Materials Transactions, 2010, 51(9): 1614−1620.

[11] HESSELBARTH H W, GOBEL I R. Simulation of recrystallization by cellular automata [J]. Acta Metallurgica et Materialia, 1991, 39(9): 2135−2143.

[12] GOETZ R L, SEETHARAMAN V. Modeling dynamic recrystallization using cellular automata [J]. Scripta Materialia, 1998, 38(3): 405−413.

[13] SHI Yu-feng, XU Qing-yan, LIU Bai-cehng. Simulation and experimental validation of three-dimensional dendrite growth [J]. Transactions of Nonferrous Metals Society of China, 2012, 22(11): 2756−2761.

[14] JIN Zhao-yang, LIU Juan, CUI Zhen-shan, WEI Dong-lai. Identification of nucleation parameter for cellular automaton model of dynamic recrystallization [J]. Transactions of Nonferrous Metals Society of China, 2010, 20(3): 458−464.

[15] RAABE D. Introduction of a scalable three-dimensional cellular automaton with a probabilistic switching rule for the discrete mesoscale simulation of recrystallization phenomena [J]. Philosophical Magazine A, 1999, 79(10): 2339−2358.

[16] RAABE D, BECKER R C. Coupling of a crystal plasticity finite-element model with a probabilistic cellular automaton for simulating primary static recrystallization in aluminium [J]. Modelling and Simulation in Materials Science and Engineering, 2000, 8(4): 445−462.

[17] RAABE D. Cellular automata in materials science with particular reference to recrystallization simulation [J]. Annual Review of Materials Research, 2002, 32(1): 53−76.

[18] DING R, GUO Z X. Coupled quantitative simulation of microstructural evolution and plastic flow during dynamic recrystallization [J]. Acta Materialia, 2001, 49(16): 3163−3175.

[19] DING R, GUO Z X. Microstructural modelling of dynamic recrystallisation using an extended cellular automaton approach [J]. Computational Materials Science, 2002, 23(1): 209−218.

[20] CHEN Fei, CUI Zhen-shan, LIU Juan, CHEN Wen, CHEN Shi-jia. Mesoscale simulation of the high-temperature austenitizing and dynamic recrystallization by coupling a cellular automaton with a topology deformation technique [J]. Materials Science and Engineering A, 2010, 527(21): 5539−5549.

[21] LIU Xiao, LI Luo-xing, HE Feng-yi, ZHOU Jia, ZHU Bi-wu, ZHANG Li-qiang. Simulation on dynamic recrystallization behavior of AZ31 magnesium alloy using cellular automaton method coupling Laasraoui–Jonas model [J]. Transactions of Nonferrous Metals Society of China, 2013, 23(9): 2692−2699.

[22] LIU Xiao, ZHU Bi-wu, LI Luo-xing. Dynamic recrystallization of AZ31 magnesium alloy simulated by Laasraoui−Jonas dislocation equation coupled cellular automata method [J]. Transactions of Nonferrous Metals Society of China, 2013, 23(4): 898−904.

[23] LEE H W, IM Y T. Numerical modeling of dynamic recrystallization during nonisothermal hot compression by cellular automata and finite element analysis [J]. International Journal of Mechanical Sciences, 2010, 52(10): 1277−1289.

[24] RUITENBERG G, WOLDT E, PETGORD A K. Comparing the Johnson–Mehl–Avrami–Kolmogorov equations for isothermal and linear heating conditions [J]. Thermochimica Acta, 2001, 378(1): 97−105.

基于元胞自动机法的 7055 铝合金动态再结晶变形参数优化

张 涛[1]，鲁世红[1]，吴运新[2]，龚 海[2]

1. 南京航空航天大学 机电学院，南京 210016；
2. 中南大学 机电工程学院，长沙 410083

摘 要：为了研究 7055 铝合金在热压缩过程中的组织演变规律，基于元胞自动机法(CA)建立 7055 铝合金动态再结晶(DRX)模型。为了获得模型的材料参数，进行单道次热压缩实验，通过最小二乘法拟合获得 7055 铝合金的位错密度模型、形核率模型和再结晶晶粒长大模型。研究应变、应变速率、变形温度和初始晶粒尺寸对热压缩过程中显微组织演变的影响。结果表明：在热压缩过程中，动态再结晶使材料晶粒明显细化。大应变、高温和低应变速率有利于晶粒细化；动态再结晶晶粒的稳态晶粒尺寸与初始晶粒大小无关，而取决于温度和应变速率的变化；分析热压缩过程动态再结晶动力学规律。由 CA 仿真流变应力值和仿真组织图与实验结果的对比可知，所建立的基于 CA 法的动态再结晶模型能有效地预测 7055 铝合金在热变形过程中的动态再结晶组织演变规律。

关键词：7055 铝合金；元胞自动机；动态再结晶；热压缩；晶粒细化

(Edited by Wei-ping CHEN)